**Atmospheric
Chemistry
and Physics
Discussions**

Numerical simulation of tropospheric injection of biomass burning products by pyro-thermal plumes

C. Rio[1]**, F. Hourdin**[1]**, and A. Chédin**[2]

[1]Laboratoire de Météorologie Dynamique, IPSL, UPMC, 75252 Paris, France
[2]Laboratoire de Météorologie Dynamique, IPSL, Ecole Polytechnique,
91128 Palaiseau, France

Correspondence to: C. Rio (catherine.rio@lmd.jussieu.fr)

ACPD

9, 18659–18705, 2009

**Modelling of
pyro-convection**

C. Rio et al.

Title Page

Abstract	Introduction
Conclusions	References
Tables	Figures

| ◄◄ | ►► |
| ◄ | ► |

| Back | Close |

Full Screen / Esc

Printer-friendly Version

Interactive Discussion

Abstract

The thermal plume model, a mass-flux scheme originally developed to represent the vertical transport by convective structures within the boundary layer, is adapted to the representation of plumes generated by fires, with the aim of estimating the height at which fire emissions are actually injected in the atmosphere. The parameterization, which takes into account fire characteristics, the induced excess of near surface temperature and mixing with environmental air, is first evaluated on two well-documented fires. Simulations over Southern Africa performed with the general circulation model LMDZ over one month show that the CO_2 can be injected far above the boundary layer height, leading to a daily excess of CO_2 in the mid-troposphere of an order of 2 ppmv. These results agree with satellite retrievals of a diurnal cycle of CO_2 in the free troposphere over regions affected by biomass burning in the Tropics.

1 Introduction

Biomass burning is a significant source for a number of atmospheric trace species. Because a fire is thermodynamically active, the vertical distribution of fire emissions depends on both its characteristics and on the meteorological environment (Kahn et al., 2007). The representation of the vertical transport of emissions above fires is a concern for the purpose of global modelling of the atmospheric composition. However, it is rarely taken into account in General Circulation Models. Here, we propose a parameterization for the convective plumes generated by the excess of buoyancy associated with biomass burning and use it to simulate the transport of CO_2 from fires over Southern Africa. This study was initially motivated by satellite retrievals from Chédin et al. (2005) suggesting a strong diurnal cycle of carbon dioxide concentration over regions affected by biomass burning, well above the planetary boundary layer. Chédin et al. (2008) show that the amplitude of this so-called Daily Tropospheric Excess (hereafter DTE) of CO_2 is highly correlated with Van der Werf et al. (2006) estimates of the CO_2

emissions from biomass burning. The retrieval being sensitive to the mean CO_2 concentration in the mid-to-upper part of the troposphere, Chédin et al. (2005) and Chédin et al. (2008) allocate this observed excess of CO_2 to a rapid uplift during the day of fire emissions – which peaks around 15:00 LT (Giglio, 2007) – to the upper troposphere.

5 The question we try to answer here is whether the vertical transport of fire emissions due to fire induced convection, so called "pyro-convection", may explain this observed diurnal cycle.

Plumes generated by an excess of temperature induced by biomass burning have already been observed to reach the stratosphere in mid and high latitudes (Fromm and

10 Servranckx, 2003; Jost and al., 2004). Such plumes are associated with "pyro-clouds", resulting from condensation inside the plume. The conjunction of several factors can explain such a high penetration of fire plumes: the density of fuel available (dense forests), the weak inversion at the top of the boundary layer and the occurrence of meteorological convective systems. In the Tropics, the conditions are less favourable,

15 atmospheric conditions during the fire season being quite dry and stable with a strong inversion at the top of the boundary layer, and predominant vegetation consisting in woodlands and grasslands. However, Coheur et al. (2007) report emissions from a young plume in the upper troposphere over Tanzania, while the ECMWF forecast model nudged with GFEDv2 emissions simulate high CO_2 concentration above 500 hPa over

20 Southern Africa (Kaiser et al., 2009). Freitas et al. (2007) propose a model of pyro-convection used in combination with a regional circulation model. In the latter study, the model for pyro-convection is used "off-line" to deduce a minimal and a maximal injection height from fire characteristics and synoptic conditions, between which gases are then uniformly emitted and transported by the 3-D model. They simulate maximal

25 injection heights of an order of 10 km in Southern America and of 7 km in Southern Africa. Using the same model, Guan et al. (2008) show that the representation of pyro-convection is necessary to reproduce the observed concentration of CO over South Africa during SAFARI 2000 by lifting CO directly in the mid-troposphere. Those recent studies confirm that emissions from biomass burning can be injected directly above the

boundary layer, even in Southern Africa during the dry season. However, refined observations of fire plumes and emissions are still missing at regional scale. Occasionaly, such observations are performed in the framework of field campaign, like SAFARI in 2000 over South Africa or more recently the AMMA (African Monsoon Multidisciplinary Analysis) program. Chédin et al. (2009) have recently refined their analysis of satellite-retrieved CO_2 columns over Southern Africa, confirming the tight relationship existing between the DTE signal and CO_2 emissions from biomass burning at regional scale.

In order to study the impact of pyro-convection on the CO_2 distribution at global scale, we adapted a mass-flux scheme originally developed to represent convective processes in the atmospheric boundary layer, the thermal plume model (Hourdin et al., 2002; Rio and Hourdin, 2008), to the representation of convective plumes induced by biomass burning. The "pyro-thermal plume model" presented here computes the vertical profiles of temperature, humidity and emitted gases along pyro-plumes given environmental conditions, CO_2 and heat flux released. The model thus provides the vertical distribution of the effective injection of biomass burning products in the atmosphere.

This paper is organized as follows. The development of the "pyro-thermal" plume model from the existing thermal plume model is first described in Sect. 2. The pyro-thermal plume model is then qualitatively evaluated on two well-documented fires either from observations (Stocks et al., 1996) or from previous studies performed with explicit simulations of fire plumes (Trentmann et al., 2006; Luderer et al., 2006). The impact of pyro-convection on the CO_2 distribution at regional scale is investigated in Sect. 4, using the General Circulation Model LMDZ (Hourdin et al., 2006), focusing on July over Southern Africa. Conclusions are drawn in Sect. 5.

2 The pyro-thermal plume model

2.1 Idealization of a fire

In the pyro-thermal plume model, a fire is characterized by two parameters: an instantaneous active burning area and an associated heat flux released. For the sake of simplicity, we consider a rectangular active fire of width L, depth d and surface $S = Ld$ as illustrated in Fig. 1. The back and front of the fire are assumed to propagate at the same constant velocity v so that the total area burned Σ_{tot} during the lifetime T of the fire is $\Sigma_{tot} = LvT$. The heat released by combustion (E in $J\,m^{-2}$) after the passing of the active fire is the product of the density of biomass burned ω (in $kg\,m^{-2}$) by the combustion heat C (in $J\,kg^{-1}$): $E = C\omega$. The averaged heat flux F (in $J\,kg^{-1}\,m^{-2}$) released by the active part of the fire is related to E by:

$$SFT = \Sigma_{tot}E \tag{1}$$

so that we have:

$$F = \frac{\Sigma_{tot}E}{ST} = \frac{Ev}{d} \tag{2}$$

2.2 Model equations

The parameterization for pyro-convection is adapted from the "thermal plume model" developed initially to represent coherent structures of the convective boundary layer (Hourdin et al., 2002; Rio and Hourdin, 2008). The thermal plume model is a mass-flux scheme, which computes vertical profiles of water, temperature and velocity inside a plume generated by a buoyancy excess near the surface, given some assumptions about the geometry of the plume and the mixing between the plume and its environment. Each atmospheric column is divided into a mean ascending thermal plume of mass flux $f = \alpha \rho w_u$ (where ρ is the air density, α the fractional cover of the plume

Modelling of pyro-convection

C. Rio et al.

Title Page

Abstract | Introduction

Conclusions | References

Tables | Figures

◄ | ►

◄ | ►

Back | Close

Full Screen / Esc

Printer-friendly Version

Interactive Discussion

and w_u the vertical velocity), and a compensating subsidence in the environment of mass-flux $-f$ as illustrated in Fig. 2.

The conservation of mass relates the vertical variation of f to the entrainment rate of air mass inside the plume e and the detrainment rate of air mass from the plume d:

$$\frac{\partial f}{\partial z} = e - d \tag{3}$$

Assuming stationarity, the plume properties are computed from:

$$\frac{\partial f \Psi_u}{\partial z} = e \Psi_e - d \Psi_u \tag{4}$$

where ψ is a conserved quantity and subscript 'u' stands for the updraft and "e" for the environment. As in classical mass-flux parameterizations of deep convection, the assumption is made that environmental values are equal to large scale values ($\psi_e = \psi$). This conservation equation is applied to total water r_t, liquid potential temperature θ_l and CO_2 concentration. The plume vertical velocity is computed from the conservation of momentum in stationary and frictionless conditions:

$$\frac{\partial f w_u}{\partial z} = -d w_u + \alpha g \gamma \tag{5}$$

where

$$\gamma = g \frac{\theta_{vu} - \theta_{ve}}{\theta_{ve}} \tag{6}$$

is the plume buoyancy, θ_v being the virtual potential temperature.

To close the system of equations, once mixing rates have be specified, an equation for the mass-flux at the base of the plume is still missing. In the thermal plume model, the closure relates the maximal velocity inside the plume to the horizontal convergence of air in the surface layer. Here, the closure is modified to compute the mass-flux at the base of the plume from fire characteristics as explained in the following section.

Modelling of pyro-convection

C. Rio et al.

Printer-friendly Version

Interactive Discussion

2.3 Initialization of the pyro-thermal

The pyro-plume is initialized in the first model layer, the top of which is located in our simulations around $H = 70$ m. Turbulence in the first model layer is illustrated in Fig. 2. Small-scale turbulence and coherent structures are both active in that layer.

5 We assume that below an height h diffusion is dominant, while above h the transport becomes more organized and is mostly carried out by convective cells. Below h, we assume a flux of the form:

$$\rho \overline{w'\theta'} = \frac{K(\theta_s - \theta_h)}{h} \tag{7}$$

where K is a diffusion coefficient and θ_s the surface potential temperature. Above

10 h, the flux is computed from plume properties, which are initiated by the temperature excess and the positive vertical velocity induced by fires in layer H, the computation of which is explained in the following.

In layer H, we assume that the area covered by the plume is constant and that the virtual potential temperature in the environment of the plume is homogeneous. At

15 height H, the heat flux F released by the fire is $F = \rho C_p w \theta'_0$, where θ'_0 is the excess of θ_v inside the plume and C_p is the air specific heat. In the absence of entrainment, the vertical component of the momentum equation (Eq. 5) is:

$$\frac{\partial f w}{\partial z} = g \alpha \rho \frac{\theta'_0}{\theta_{ve}} \tag{8}$$

As the surface covered by the plume is constant in layer H, Eq. (8) becomes (ne-

20 glecting the variations of ρ):

$$\frac{\partial w^2}{\partial z} = g \frac{\theta'_0}{\theta_{ve}} = g \frac{F}{\rho C_p w \theta_{ve}} \tag{9}$$

Thus

$$\frac{2}{3}\frac{\partial w^3}{\partial z} = \frac{gF}{\rho C_p \theta_{ve}} \tag{10}$$

from which we deduce the vertical velocity at H:

$$w(H) = w_0 = \left(\frac{3gFH}{2\rho C_p \theta_{ve}}\right)^{1/3} \tag{11}$$

The temperature excess θ_0' induced by the fire in layer H is finally:

$$\theta_0' = \frac{F}{\rho C_p w} = \left(2\frac{(\frac{F}{\rho C_p})^2 \theta_{ve}}{3gH}\right)^{1/3} \tag{12}$$

We find that w_0 scales with $F^{1/3}$ and θ_0' with $F^{2/3}$, a dependence also established by Freitas et al. (2007).

The plume is thus initialized at the top of the first model layer by θ'_0 from Eq. (12) and a mass-flux $f = \alpha \rho w_0$ with $\alpha = S/S_m$ where S_m is the area of the model grid cell. Note that this initialization does not depend on the K coefficient or h, which only control the surface temperature excess $\theta_s - \theta_h$, which could be deduced from θ'_0 making further assumptions.

2.4 Specification of mixing rates

Due to boundary layer turbulence, potential temperature in the environment of the fire is well-mixed above the surface layer, up to a specific height that corresponds to the minimum of virtual potential temperature flux. In this mixed layer, we assume, like we did below H, that the surface covered by the pyro-plume is independent of height, so that the acceleration of air due to the large buoyancy of fire air parcels is associated

with a large lateral entrainment of environmental air (as $\alpha = \frac{f}{\rho w_u}$). This convergence of air explains the fast decrease of temperature with height commonly observed above fires. If we suppose that $\alpha\rho$ rather than α is constant within the mixed layer, in the absence of detrainment, Eq. (5) leads to:

$$\alpha\rho \frac{\partial w_u^2}{\partial z} = \alpha\rho\gamma \tag{13}$$

The entrainment needed to keep the fraction constant in the mixed layer is thus:

$$e = \frac{\partial f}{\partial z} = \alpha\rho \frac{\partial w_u}{\partial z} = \frac{\alpha\rho}{2w_u} \frac{\partial w_u^2}{\partial z} = \frac{\alpha\rho}{2w_u}\gamma \tag{14}$$

Detrainment in the mixed layer is specified considering that the plume is eroded with a mixing length λ:

$$d = \frac{\partial}{\partial z}(\frac{\alpha\rho w_u \sqrt{\lambda z}}{l}) \tag{15}$$

where l is a characteristic length of the fire geometry, defined as $\sqrt{(S)}$. We take $\lambda = 30\,m$ as in the original version of the scheme.

Above the mixed layer, and inside pyro-clouds, entrainment and detrainment rates are specified for simplicity as constant fractions of the mass-flux, a classical formulation derived from explicit simulations of shallow convection (Siebesma and Holtslag, 1996):

$$d = \delta f \tag{16}$$

$$e = \epsilon f \tag{17}$$

In the thermal plume model of Rio and Hourdin (2008), $\delta = 0.002\,\text{m}^{-1}$ and $\epsilon = 0.0008\,\text{m}^{-1}$, values deduced from simulations of shallow cumulus. However, mixing rates should probably be an order of magnitude lower for deep than for shallow

Modelling of pyro-convection

C. Rio et al.

Title Page

Abstract | Introduction

Conclusions | References

Tables | Figures

|◄ | ►|

◄ | ►

Back | Close

Full Screen / Esc

Printer-friendly Version

Interactive Discussion

convection (Tiedtke, 1989; Siebesma and Holtslag, 1996). As pyro-convection can be either shallow or deep, we make ϵ and δ inversely proportional to a characteristic dimension of the plume, taken as $\sqrt{(S)}$, so that the larger the plume, the smaller the mixing. Detrainment is larger than entrainment and we have $\epsilon = \beta \delta$ with $\delta = 1/\sqrt{(S)}$ and $\beta = 0.4$.

3 Evaluation of the scheme on two well-documented fires

For evaluation of the pyro-thermal plume model we first simulate pyro-plumes generated by two well-documented fires: a boreal forest fire in Canada and a savanna fire in South Africa.

3.1 The Chisholm fire in Canada

The Chisholm fire occurred between the 23rd and the 29th of May 2001 in Canada and burned an area of 100 000 ha (ASRD, 2001). On the 28th of May a pyro-cloud was observed above the fire and emissions were retrieved above the tropopause, in the stratosphere (Fromm and Servranckx, 2003), located at 12 km in this region. Environmental conditions issued from ERA40 reanalysis at fire location (55N/114W) the 28th of May 2001 at 16:30 LT are illustrated in Fig. 3. The mixed layer height is estimated to be approximately 2500 m.

The plume generated by the Chisholm fire has been simulated with the 3-D mesoscale ATHAM model (Active Tracer High resolution Atmospheric Model, Oberhuber et al., 1998; Herzog et al., 1998) by Trentmann et al. (2002), Trentmann et al. (2006) and Luderer et al. (2006). The horizontal resolution used is of 100 m while the vertical resolution varies from 50 m near surface to 150 m at the tropopause. The pyro-plume is thus explicitly resolved and we use results from their simulations as a reference. From their studies we extract fire characteristics we need to initialize the pyro-thermal

Modelling of pyro-convection

C. Rio et al.

plume model. The quantity of consumed fuel is estimated to be $\omega = 76\,000\,\text{kg}\,\text{ha}^{-1}$. The speed rate at which the fire propagates is $v = 1.5\,\text{m}\,\text{s}^{-1}$. From those two variables we can deduce the power of the fire front I by the relation:

$$I = C\omega v \tag{18}$$

where C is the combustion heating rate ($C \approx 17\,781\,\text{kJ}\,\text{kg}^{-1}$). Trentmann et al. (2006) consider a fire front 15 km large and 300 m deep. From this depth d of the fire front we can deduce the heat flux released by the fire $F = I/d$. Thus, for the Chisholm fire, we obtain $I = 202\,703\,\text{kW}\,\text{m}^{-1}$ and $F = 675\,\text{kW}\,\text{m}^{-2}$. As suggested by Luderer et al. (2006), 50% of this heat flux is assumed to be effectively used for convection, the other half for radiation. However this distribution is still subject to discussions.

Characteristics of the plume simulated by the pyro-thermal plume model for a heat flux $F = 337.5\,\text{kW}\,\text{m}^{-2}$ and an active burning area $S = 4.5\,\text{km}^2$ are represented in Fig. 4. Main features are compared in Table 1 with values extracted from Trentmann et al. (2006) (values are approximately deduced from their Figs. 10 and 11). An excess of temperature of an order of 40 K, as a maximal vertical velocity of $40\,\text{m}\,\text{s}^{-1}$ are obtained, in consistency with results from Trentmann et al. (2006), even if the evaluation of the scheme stays rough at this stage. However, the simulated injection height, even if it is too low (slightly more than 10 km), does not allow emissions to reach the stratosphere located at 12 km.

3.2 Fire in the Kruger National Park in South Africa

We now consider a savanna fire that took place in the Kruger National Park in South Africa during the SAFARI campaign in 1992. Environmental conditions from ERA40 reanalysis at fire location (25 S/31 E) the 24th of September 1992 at 14:00 LT are shown in Fig. 3. The inversion at the top of the boundary layer is much stronger than for the Chisholm fire. The mixed layer is estimated to be around 1500 m.

Results are more difficult to evaluate because vertical characteristics of the convective plume are not referenced. However, Stocks et al. (1996) report a plume reaching

Modelling of pyro-convection

C. Rio et al.

⏮   ⏭

◄   ►

Back   Close

Full Screen / Esc

Printer-friendly Version

Interactive Discussion

about 2717 m just before 14:00 LT with a small cumulus at the top. They estimate the density of savanna burned to 3786 kg ha^{-1}. The fire lasted several hours, devastating 2333 ha. The propagating rate is estimated to be 1.62 m s^{-1} (Stocks et al., 1996). From those characteristics, we can deduce the intensity of the fire front $I = 10\,906$ kW m^{-1} for d≈700 m and a heat flux $F = 15.6$ kW m^{-2} (50% of which is assumed to be available for convection). As can be noted, those values are far weaker than those related to the boreal forest fire in Canada. Plume characteristics obtained with those definitions and an estimated active burning surface of 1 km^2 are represented in Fig. 5.

The excess of virtual potential temperature is of 3.1 K in the first model layer, more than ten times weaker than for the Chisholm fire. This excess is of 2 K at 1000 m and becomes negative above 2000 m, where the vertical velocity is maximal and of 12 m s^{-1}. No pyro-cloud form above the fire and the thermal plume reaches 3300 m. Comparing with observations from Stocks et al. (1996), the plume height is 600 m too high, with no cumulus cloud at the top.

3.3 How to explain discrepancies?

These tests of the pyro-thermal plume model on two different cases, a pyro-plume reaching the stratosphere in boreal regions and a plume being trapped in the boundary layer in South Africa, bring into evidence some differences between results and observations which can have several sources. First, the plume initiation is controlled by fire characteristics, the heat flux available for convection and the active burning area, on which large uncertainties still remain. Second, the thermal plume model has been initially developed to represent shallow plumes induced by an excess of temperature of the order of 1 K. It is thus used here in configurations for which the scheme has not been intially developed for, possibly leading to deep convection. As mixing intensity is different whether convection is shallow or deep, we modified the definitions initially prescribed for shallow convection by chosing a formulation depending on plume dimensions, potentially adapted to both shallow and deep convection. However, this intermediate formulation may explain the problem of the underestimation of the plume

height generated by the Chisholm fire and the overestimation of the plume height generated by the Kruger fire. We also neglected the water release in the plume by biomass burning. Sensitivity tests on all these parameters are performed in the next section.

3.4 Sensitivity to fire characteristics and scheme parameters

3.4.1 Sensitivity to fire characteristics

Injection heights obtained by varying either the heat flux released or the active burning area are represented in Fig. 6 for the two environmental conditions of the Chisholm fire and the Kruger fire. In the boreal conditions of the Chisholm fire, there is a sharp transition from plumes confined in the mixed layer to plumes reaching 10 km when the heat flux released increases from $5\,kW\,m^{-2}$ to $20\,kW\,m^{-2}$ for an active burning surface of $4.5\,km^2$, or when the active burning area increases from $0.4\,km^2$ to $1\,km^2$ for a heat flux released of $337.5\,kW\,m^{-2}$. In the conditions encountered in the Kruger National Park, the evolution of the injection height depending on the heat flux released is more continuous. However, if the heat flux could reach values encountered in boreal regions, the injection height would reach $7000\,m$ in such conditions. Such injection height can also result from very large fire fronts ($10\,km^2$) for realistic heat flux in that region.

The injection height is thus sensitive to both environmental conditions and fire characteristics. However, in a reasonable range of estimated values of the heat flux and of the active burning area in the cases of the Chisholm fire and the Kruger fire, the simulated injection height does not vary significantly.

Tests are also performed by releasing F_q=0.5 kg of water per kg of burned fuel at the base of the plume. The excess of total water q'_0 in layer H is then computed from:

$$q'_0 = \frac{F_q}{\rho w_0} \tag{19}$$

For the Chisholm fire, the injection height increases from 10 230 to 10 370 m and for the Kruger fire from 3370 to 3400 m. As already mentionned by Luderer et al.

(2006), taking into account the water released by the biomass burned seems to have no significant impact on the injection height.

3.4.2 Sensitivity to scheme parameters

As already mentionned, mixing with environmental air plays a major role in convec-
tion dynamics. Entrainment in particular drives the plume characteristics. The sen-
sitivity of the injection height to $\beta = e/d$ is given in Fig. 6 (left). For the Chisholm
fire, $e/d = 0.1$ allows to simulate a plume reaching 12 km, while for the Kruger fire,
$e/d = 0.8$ leads to an injection height lower than 3 km, in better agreement with obser-
vations. Thus, $e/d = 0.1$ seems to be better suited for deep plumes while $e/d = 0.8$
for shallow plumes. This point deserves further investigations, however $e/d = 0.4$ is an
intermediate value which allows to obtain satisfactory results for the two very different
cases considered here.

The sensitivity of the injection height to the parameter λ controlling the detrainment in
the mixed layer is weak (not shown). Here we keep $\lambda = 30\,m$ as in the original thermal
plume model.

Even if there are some discrepancies between model results and observations or
high resolution simulations available for the Chisholm fire and the SAFARI fire in the
Kruger National Park, the pyro-thermal plume model proposed here is able to repro-
duce the main features of the pyro-plumes in those two cases and is thus appropriate
to simulate injection heights for a large range of conditions. In the next section, the
scheme is used to evaluate injection heights and CO_2 transport at regional scale over
Southern Africa.

4   Application to pyro-plumes in Southern Africa and to their impact on the diurnal cycle of CO_2 in the free troposphere

4.1   The diurnal cycle of fire characteristics

Several studies report that the normalized frequency of fires follows a strong diurnal cycle, active fire pixels being maximum in mid-afternoon (Giglio, 2007; Justice et al., 2002). Here we assume that this diurnal cycle is close to a Gaussian centered around 15:45 LT with a standard deviation of 1 h. This Gaussian function is used to specify the diurnal evolution of fire heat flux and related CO_2 emissions. The instantaneous heat flux F and flux of CO_2 released by fires F_{CO_2} are thus specified by:

$$F(t) = \overline{F}N(t) \tag{20}$$

and

$$F_{CO_2}(t) = \overline{F_{CO_2}}N(t) \tag{21}$$

where $\overline{X} = \frac{1}{T}\int_0^T X(t)dt$, T being the duration of one day and N the normalized Gaussian centered around 15:45 LT and of standard deviation $\sigma = 1$ h ($\overline{N} = 1$).

Typical values for $\overline{F}$ and $\overline{F_{CO_2}}$ encountered in Southern Africa need to be specified. Korontzi et al. (2003) estimate that in semi-arid regions, 60% of the total area burned is related to 3% of the fires, those burning more than 100 km^2, while 43% of fires burn less than 1 km^2, devastating only 2% of the total area burned in those regions. The larger fires are thus the less frequent, but are responsible for most of the emissions, and for the most intense pyro-plumes. This is why we will consider such fires in the following. During the dry season 1989, Barbosa et al. (1999) report a total burned area over the season of 1 541 000 km^2 for 456 Tg of biomass burned. This corresponds to a density of biomass burned of 2960 kg ha^{-1}. If we consider a propagation rate of 1.5 m s^{-1}, the fire front intensity is $I = 7894$ kW m^{-1}, which corresponds to a heat flux

$F = 78 \, \text{kW m}^{-2}$ for a front depth $d = 100 \, \text{m}$ or $F = 39 \, \text{kW m}^{-2}$ for $d = 500 \, \text{m}$. Values for F of dozens of kW m^{-2} seem reasonable, an intermediate value between the Chisholm fire and the Kruger fire. For simplicity, the active burning area of a fire is kept constant during the day, and we take $S = 2 \, \text{km}^2$. The integration of Eq. (1) in time gives:

$$S \int_0^T F(t) dt = \Sigma_{\text{tot}} E \qquad (22)$$

so that we have:

$$\overline{F} = \frac{\Sigma_{\text{tot}} E}{ST} \qquad (23)$$

We consider a maximum value for F of $80 \, \text{kW m}^{-2}$. $\overline{F_{\text{CO}_2}}$ is given by the map of emissions displayed in Fig. 7, derived from observations performed in the framework of the AMMA field campaign during July 2006 (Liousse et al., 2009).

4.2 Set up of 3-D simulations

Simulations are performed with the standard version of LMDZ (Hourdin et al., 2006) with an horizontal grid made of 96 points equally distributed from pole to pole and 72 points in longitude, a vertical resolution of 40 layers over the entire atmospheric column and a time step of 90 s for a typical month of July. The model includes parameterizations of boundary layer turbulence (Louis, 1979), deep convection (Emanuel, 1991), clouds (Bony and Emanuel, 2001) and radiation (Morcrette, 1984). Two types of simulations are conducted: a reference simulation with the standard version of LMDz in which CO_2 emissions are injected uniformly in the first model layer (REF), and a simulation in which the pyro-thermal plume model is activated (TH) and emissions are injected at the base of the pyro-thermal. In that case, the flux of CO_2 at level H must equal the surface flux of CO_2. The concentration of CO_2 at the base of the plume is

Modelling of pyro-convection

C. Rio et al.

Title Page

Abstract | Introduction

Conclusions | References

Tables | Figures

◀◀ | ▶▶

◀ | ▶

Back | Close

Full Screen / Esc

Printer-friendly Version

Interactive Discussion

thus:

$$q_{CO_2}(t) = \frac{F_{CO_2}(t)}{\alpha \rho w_0(t)} \qquad (24)$$

4.3 Injection heights

The simulated injection height varies in space and time as it depends on the heat flux
and environmental conditions. The maximal injection height computed over the 20 last
days of July with simulation TH is represented in Fig. 8 (left). The maximal simulated
injection height varies from 2500 m in the East to 6000 m in the center of the continent
and reaches 7500 m in the south-west of the considered region.

This maximal injection height is compared with the mean injection height reached
when emissions pass the boundary layer height and with the mean boundary layer
height in Fig. 8 (middle), where heights are averaged between 5 S and 20 S. The
boundary layer height is located around 2–3 km. When emissions are directly injected
above the boundary layer, they reach in average 4 km and can sometimes be lifted
higher up to 7 km. The percentage of times for which, the injection height passing
2 km, it is finally larger than 4 km is represented in Fig. 8 (right). Those results show
that part of fire emissions from intense fires in the Tropics can be directly injected above
the boundary layer in the free troposphere, and in more than 30% of cases directly be-
tween 4 and 7 km over the South-West part of Southern Africa.

4.4 CO_2 transport at global scale

The vertical distribution of CO_2 averaged over the 20 last days of July between 5 S
and 20 S is represented in Fig. 9 for simulations REF (left) and TH (middle). The
activation of the pyro-thermal plume model mainly affects the vertical distribution of
CO_2 over Southern Africa. When emissions are injected in the first model layer, the
concentration is maximal near surface and decreases above boundary layer top. When
the pyro-thermal plume model is activated, the maximal concentration is located around

Full Screen / Esc

Printer-friendly Version

Interactive Discussion

700 hPa so that the concentration within the boundary layer is less and emissions are spread farther to the east at higher levels. The peak of the CO_2 concentration vertical distribution is also shown for those simulations in Fig. 10 for the region from 60 W to 60 E and 30 S to 10 N. This figure confirms that CO_2 is transported farther to the north in the REF simulation and farther to the east in the TH simulation.

As illustrated in the right panels of Fig. 9 and Fig. 10, where results are displayed for a simulation in which $\beta = e/d = 0.1$, the CO_2 vertical and horizontal distribution may also depend on the specification of mixing between the plume and the environment which determines the heights where CO_2 from the plume is detrained into the troposphere. This modifies the mass-flux and then both entrainment and detrainment at each level. With $\beta = 0.1$, less CO_2 is detrained at low levels, where easterlies are dominant, which explains the difference of the CO_2 distribution over the Atlantic Ocean. More CO_2 is detrained at higher levels, between 600 and 500 hPa, where it is transported down eastward. Those results illustrate how the scheme could be further evaluated, for example to specify the value of β, from observations of CO_2 concentration in that region.

4.5 Diurnal cycle of CO_2 in the troposphere

The pyro-thermal plume model is now used to investigate the potential impact of pyro-plumes on the diurnal cycle of CO_2 in the free troposphere. A vertical section of the amplitude of the simulated diurnal cycle of CO_2 (difference between 19:30 LT and 07:30 LT) averaged between 5 and 20S and over the 20 last days of July is represented in Fig. 11 for simulations REF (left) and TH (right). In the reference simulation, the CO_2 evening excess is maximal near the surface in a range between 4 and 8 ppmv. Above, the signal decreases and vanishes around 800 hPa. When the pyro-thermal plume model is activated, the signal has two maximal values, one near the surface of about 1 ppmv and another around 700 hPa, reaching 3 ppmv. This maximum is related to CO_2 being rapidly transported from the surface and detrained from pyro-clouds.

Those results can be explained by the following "back of the enveloppe" estimation of

the atmospheric CO_2 concentration increase due to fires and the corresponding diurnal cycle. The fire induced convection introduces a vertical distribution function (I) for the effective injection of CO_2, so that the daily increase of CO_2 over one day due to fire emissions alone at pressure level p reads:

$$\epsilon(p) = \lambda F_{CO_2} \delta t I(p) \tag{25}$$

where λ is the factor converting the flux of CO_2 into a concentration of CO_2 (in ppmv):

$$\lambda = \frac{g}{P_s} \frac{\mu_{air}}{\mu_{CO_2}} \tag{26}$$

P_s being the surface pressure and

$$\frac{1}{P_s} \int I(p) dp = 1 \tag{27}$$

Starting from a CO_2 free atmosphere, the CO_2 concentration in the region of fires will build up days long under fire emissions, until an averaged balance is reached between daily CO_2 injection ϵ and daily ventilation by large-scale advection. This latter term is of the order of $-\frac{V\delta t}{L} CO_2^{eq}$, V being a typical wind speed, L the size of the source region and CO_2^{eq} the CO_2 concentration at equilibrium, so that:

$$CO_2^{eq} = \frac{\epsilon L}{V \delta t} \tag{28}$$

Half of the ventilation occurs during the night, so that the evening minus morning difference of CO_2 concentration equals $\frac{V\delta t}{2L} CO_2^{eq} = \epsilon/2$. As a first approximation, we can expect the evening minus morning difference of CO_2 concentration to be half the concentration increase per day due to biomass burning emissions without considering any ventilation. Note that this means that this evening excess of CO_2 does not depend on the large-scale circulation, but only on the increase of CO_2 concentration per day. This relationship between the evening minus morning difference of CO_2 concentration and

Modelling of pyro-convection

C. Rio et al.

the daily CO_2 injection, as well as the role of the large-scale circulation, are illustrated more explicitly on a 1-D and a 2-D ideal cases in the Appendix A.

As a first estimation, let us consider a source of $1000\,\mathrm{g\,m^{-2}}$ month^{-1} ($\approx 30\,\mathrm{g\,m^{-2}}$ day^{-1}) which injects CO_2 between 07:30 LT and 19:30 LT in a layer 300 hPa deep. In that layer, we get an increase of CO_2 in one day of $\epsilon = 6.5$ ppmv. The evening minus morning difference of CO_2 in that layer will then be of an order of $\epsilon/2 = 3.25$ ppmv. This value is close to the maximum obtained around 700 hPa with simulation TH (Fig. 11).

4.6 Simulation of the satellite retrieved Daily Tropospheric Excess

The previous estimation considers the effective amount of CO_2 released to the atmosphere. However, observations of the DTE are sensitive to only a part of the atmosphere as illustrated by the weighting function in Fig. 12 (after Chédin et al., 2003). The observed DTE is thus the vertically integrated evening minus morning difference obtained with the weighting function (W), so that:

$$\mathrm{DTE} = \frac{1}{P_s} \int_{ps}^{0} (CO_{2_{07:00\,\mathrm{p.m.}}} - CO_{2_{07:00\,\mathrm{a.m.}}}) W(p) dp \qquad (29)$$

Observations of the DTE signal in July is represented in Fig. 13 (after Chédin et al., 2008). It reaches 3 ppmv over Southern Africa. The simulated DTE obtained with simulations REF and TH are displayed in Fig. 14. In simulation REF, an excess of CO_2 of a few 0.1 ppmv is obtained around 5 N and around 10 S, while a deficit of CO_2 is obtained around 5 S, both over land and ocean. The signal obtained in the Northern Hemisphere in simulation REF may be related to the diurnal cycle of deep convection which is very active in the Northern Hemisphere in that season. As already seen in Fig. 10, emissions are transported farther to the north in simulation REF, where they can be transported to still upper levels by deep convection. In simulation TH, results are much closer to observations. As observed, the largest signal is obtained over the

region where CO_2 was emitted. The restriction of the signal over a specific region is due to the averaging over several days. Indeed, a DTE signal is also obtained daily in each simulation over other regions, particularly over ocean. But due to different advection scales, the DTE signal is not at the same location from day to day so that the averaged

5   results give a DTE signal only significant over the region where it is most persistent. The analysis of the simulated daily DTE versus observations is further shown in Chédin et al. (2009). Those results confirm that the DTE signal can be attributed to the diurnal cycle of fire activity, with CO_2 being transported from the surface to levels above the boundary layer height along the day.

10   The DTE signal can also be directly estimated from biomass burning CO_2 emissions using the previous derivation for which CO_2 is uniformly emitted between 800 and 500 hPa:

$$\text{DTE} = \frac{1}{P_s} \int_p \frac{\epsilon}{2} W(p) dp = F_{CO_2} \delta t \frac{g}{2P_s} \frac{\mu_{\text{air}}}{\mu_{CO_2}} \Gamma \tag{30}$$

where Γ is a factor defined from the vertical distribution function of fire emissions and

15   the weighting function:

$$\Gamma = \frac{1}{P_s} \int I(p) W(p) dp \tag{31}$$

If we consider that $I(p) = 1$ between 500 and 800 hPa and 0 elsewhere, we get $\Gamma_{650} = 0.31$ and the DTE signal obtained from CO_2 emissions is displayed in Fig. 14 (right). The spatial distribution of the DTE obtained is quite close to the simulated one

20   with simulation TH, even if the approach used does not allow to reproduce a signal out of the source region which can occur due to the existence of preferential wind direction.

The DTE signal is between 0.5 and 1 ppmv over the source region. This value is still lower than the 3 ppmv observed by Chédin et al. (2005, 2008). This difference can be due to several uncertainties in both observations and modelling. Equation (30)

25   allows to distinguish three different sources of uncertainties: those relying on CO_2

Modelling of pyro-convection

C. Rio et al.

Printer-friendly Version

Interactive Discussion

emissions from biomass burning (F_{CO_2}), those relying on the vertical distribution of those emissions in the atmosphere (the function I simulated, for example, by the pyro-thermal plume model), and those relying on the derivation of the weighting function of satellite observations. Large uncertainties still rely on CO_2 emissions from biomass burning, which are deduced from several variables independently evaluated, among them the burning area. In addition, the simulation performed here corresponds to July 2006 while the observed signal is averaged between 1987 and 1990. The difference could thus be due to interannual variability of CO_2 emissions. Concerning the pyro-thermal plume model, the simulated vertical distribution of CO_2 emissions strongly depends on the prescribed mixing rates between the plume and its environment. This point has to be investigated further in the future using observations and high resolution simulations of pyro-plumes. Uncertainties of an order of $50\,hPa$ may also affect the location of the peak of the weighting function of satellite observations. Of course the maximum DTE signal would be obtained in case the peaks of the distributions I and W coincide. By shifting the peak of the vertical distribution of CO_2 concentration I from 650 to $350\,hPa$, we get: $\Gamma_{550} = 0.47$, $\Gamma_{450} = 0.57$ and $\Gamma_{350} = 0.64$ leading to a factor 2 on the DTE signal obtained. Note that part of the differences between the simulated and observed DTE could also come from contaminations of the retrieved DTE signal by either ozone, dust or smoke aerosols, or remaining (undetected) thin clouds, however not expected to exceed 1 ppm at that time of the year (see Chédin et al., 2009).

5 Conclusions

In the present study, the thermal plume model of Rio and Hourdin (2008) is adapted to the representation of the vertical transport by plumes generated by fires. The model computes the vertical distribution of fire emissions induced by pyro-convection given fire characteristics, burning area and heat flux released, and environmental conditions. The model is first shown to satisfactorily reproduce the characteristics of two well documented fires in boreal and tropical regions in 1-D configuration. Sensitivity tests to fire

Modelling of pyro-convection

C. Rio et al.

characteristics show that, despite less favourable conditions, emissions from tropical fires may also penetrate well above the boundary layer depending on the heat flux or burning area. Sensitivity tests to scheme parameters highlight the key role of mixing prescription between the pyro-plume and its environment. In the future, 3-D explicit simulations of large fire plumes may help validate, tune and improve the pyro-thermal plume model on those aspects.

When implemented in the LMDZ General circulation model, the pyro-thermal plume model injects directly a large fraction of fire products well above 4 km, in the region of African biomass burning. Because fire emissions occur mainly during the afternoon in this region, this produces a 2-ppmv amplitude diurnal cycle of CO_2 concentration in the mid-troposphere, as first suggested by Chédin et al. (2005) from remote sensing. The vertical integration of this evenings minus mornings CO_2 concentration using the weighting function of satellite retrieval gives a Daily Tropospheric Excess of an order from 0.5 to 1 ppmv, which is lower than the 3 ppmv obtained by Chédin et al. (2008) from observations. The discrepancy may come from the large uncertainties that remain on fire characteristics and emissions, from the vertical distribution of CO_2 above fires computed by the pyro-thermal plume model and from uncertainties on the observed DTE signal. A direct estimation of the DTE signal from CO_2 emissions is also proposed, which only depends on the vertical distribution of fire emissions and on the weighting function of satellite sensitivity, and not from large-scale advection. This estimation allows recovering simply the simulated DTE signal when assuming a vertical distribution of fire emissions.

A step further would be to take fire emissions and characteristics into account more precisely. Observations of fire emissions and of the atmospheric composition from the AMMA field campaign could be used to initialize and validate the scheme at regional scale by considering other gases like CO, O_3... Simulations could be extended to the whole globe using global maps of CO_2 emissions from biomass burning. When available, global maps of heat flux released would be very useful to compute the injection height. A promising method is the use of the Fire Radiative Power derived from satel-

lite measurements, which integration over the lifetime of a fire should be proportional to fire emissions (Wooster et al., 2005). However, such method has not been validated at regional nor at global scale yet, even if such evaluation is in progress (Schultz et al., 2008). A scheme like the pyro-thermal plume model will be very useful to understand and predict more precisely the CO_2 concentration over the globe, and help to disentangle the respective role of atmospheric transport on the one hand and of sources or sinks of CO_2 on the other hand.

Appendix A

Academic computations of DTE

Here we present two idealized cases in order to illustrate the relationship between the Daily Tropospheric Excess (DTE) of CO_2 and the daily injection of CO_2, as well as the role played by the large-scale circulation on a daily and a monthly basis. In the first case, the fire is idealized by a segment of length L emitting CO_2 from 07:00 LT to 19:00 LT. In the second case, the fire is a circle with a diameter of 3000 km.

A1   1-D computation

In the first case we consider the DTE that would be created in a 1-D world by an homogeous fire area over a segment $[0, L]$, with a constant advection with wind U. For simplicity, we assume that fires also emit CO_2 uniformly between 07:00 and 19:00 local time. We denote by ϵ the CO_2 increment over 1 day due to fire emission alone (as in the main text) and by Q the CO_2 concentration. In this simple case, $Q=0$ upstream of the fire emission (for $x<0$). In the fire emission region, the average balance in quasi steady state regime is $\epsilon = -U\delta t Q_x$ where $\delta t=1$ day, and Q_x is the spatial derivative of Q in x. Since ϵ is positive and constant within the fire area, Q must increase linearly from $x = 0$ to $x = L$, where it reaches a value $Q_L = \epsilon L/(U\delta t)$

As in our 3-D considerations, DTE=$\epsilon/2$ since half of the CO_2 sink due to advection

Modelling of pyro-convection

C. Rio et al.

occurs between 19:00 LT and 07:00 LT.

For $x > L$, the averaged CO_2 concentration stays close to Q_L. Because the concentration is $\epsilon/2$ larger for $x = L$ at 19:00 LT than at 07:00 LT, exactly the opposite will be obtain beyond the emission region at $x = L + U\delta t/2$ due to pure advection.

This result is checked numerically for L = 3000 km, a mesh δx = 100 km, U = 10 m/s and $\delta t = 10^5$ s, so that $L/(U\delta t) = 3$. Advection is computed with a simple first order upstream scheme. Tracer concentration increases on the first few days to reach a steady-state diurnal cycle. Final concentrations are shown on the left panel of Fig. 15. As expected, the concentration increases linearly with x, to reach a value slightly larger than 3. The DTE is also close to $\epsilon/2$ on the emission region with negative values for $L \simeq L + U\delta t/2$ (3500 km on the graph). So, compared with expectations, the maximum value is just slightly stronger and the DTE shows some oscillations. The oscillations are due to the fact that Q_x is in steady state on a daily basis but oscillates during the day. To confirm the dependance with L as well as the constancy of the DTE, we show a second computation for a wider domain of emission (L = 6000 km). A smoothing is also applied to the emission function so that the oscillation disapears in that case (Fig. 15, right).

A2   2-D computation

The fact that Q stays maximum downstream of the fire emission region is due to the 1-D domain. A similar simulation is performed with a 2-D code. The source region is a circle with a diameter of 3000 km. The wind speed is of U_0 = 10 m/s but oscillates from south-westerlies to north-westerlies. For the sake of simplicity, U_0 is assumed to be constant in the whole domain.

The resulting concentration for 3 particular days is shown in Fig. 16 together with the instantaneous DTE for each day. In the same figure, the fourth panel shows the averaged concentration and DTE on the last 70 days of a 100-day simulation. At a given time, as for day 50, the DTE can be quite large outside of the source region. At this particular day, the wind is shifting from south-westerlies to westerlies. The DTE

is positive north of the Q horizontal plume since the Q concentration increases there due to advection but it will also reinforce during the following night. Once again the quasi-steady state concentration in the fire region is of the order of $\epsilon L/(U\delta t) \simeq 3$ while the averaged DTE is of the order of $\epsilon/2$. In addition, while the averaged concentration is still significant downstream of the emission region, the DTE is restricted to the fire region.

Results obtained here in a 1-D and a 2-D idealized cases explain results obtained in 3-D and illustrate why the DTE signal is dependent on daily emissions, and independent on large-scale circulation.

References

ASRD: Final Documentation Report – Chisholm Fire (LWF-063), Forest Protection Division, ISBN: 0-7785-1841-8, Tech. rep., Alberta Sustainable Resource Development, 2001. 18668

Barbosa, P. M., Stroppiana, D., and Grégoire, J.-M.: An assessment of vegetation fire in Africa (1981-1991): burned areas, burned biomass, and atmospheric emissions, Global Biogeochem. Cy., 13, 933–950, 1999. 18673

Bony, S. and Emanuel, K. A.: A parameterization of the Cloudiness Associated with Cumulus Convection; Evaluation Using TOGA COARE Data, J. Atmos. Sci., 58, 3158–3183, 2001. 18674

Chédin, A., Serrar, S., Scott, N. A., Crevoisier, C., and Armante, R.: First global measurement of mid-tropospheric CO_2 from NOAA polar satellites: the tropical zone, J. Geophys. Res. Atmos., 108, 4581, doi:10.1029/2003JD003439, 2003. 18678, 18701, 18702

Chédin, A., Serrar, S., Scott, N. A., Pierangelo, C., and Ciais, P.: Impact of tropical biomass burning emissions on the diurnal cycle of upper tropospheric CO_2 retrieved from NOAA 10 satellite observations, J. Geophys. Res. Atmos., 110, D11309, doi:10.1029/2004JD005540, 2005. 18660, 18661, 18679, 18681

Chédin, A., Scott, N. A., and Armante, R.: A quantitative link between CO_2 emissions from tropical vegetation fires and the daily tropospheric excess of CO_2 seen by NOAA-10 (1987–1991), J. Geophys. Res., 113, D05302, doi:10.1029/2007JD008576, , 2008. 18660, 18661, 18678, 18679, 18681

Chédin, A. and Scott, N. A. and Ciais, P. and Rio, C. and Hourdin, F. and Crevoisier, C. and Armante, R.: Regional-scale correlation between CO_2 fire emissions, burned areas, and mid-tropospheric CO_2 daily variations over Southern Africa, Atmos. Chem. Phys., in press, 2009.

Coheur, P.-F., Herbin, H., Clerbaux, C., Hurtmans, D., Wespes, C., Carleer, M., Turquety, S., Rinsland, C. P., Remedios, J., Hauglustaine, D., Boone, C. D., and Bernath, P. F.: ACE-FTS observation of a young biomass burning plume: first reported measurements of C_2H_4, C_3H_6O, H_2CO and PAN by infrared occultation from space, Atmos. Chem. Phys., 7, 5437–5446, 2007, http://www.atmos-chem-phys.net/7/5437/2007/. 18661

Emanuel, K. A.: A scheme for representing cumulus convection in large-scale models, J. Atmos. Sci., 48, 2313–2335, 1991. 18674

Freitas, S. R., Longo, K. M., Chatfield, R., Latham, D., Silva Dias, M. A. F., Andreae, M. O., Prins, E., Santos, J. C., Gielow, R., and Carvalho Jr., J. A.: Including the sub-grid scale plume rise of vegetation fires in low resolution atmospheric transport models, Atmos. Chem. Phys., 7, 3385–3398, 2007, http://www.atmos-chem-phys.net/7/3385/2007/. 18661, 18666

Fromm, M. D. and Servranckx, R.: Transport of forest fire smoke above the tropopause by supercell convection, Geophys. Res. Lett., 30(10), 1542, doi:10.1029/2002GL016820, 2002. 18661, 18668

Giglio, L.: Characterization of the tropical diurnal fire cycle using VIRS and MODIS observations, Remote Sens. Environ., 108(4), 407–421, 2007. 18661, 18673

Guan, H., Chatfield, R. B., Freitas, S. R., Bergstrom, R. W., and Longo, K. M.: Modeling the effect of plume-rise on the transport of carbon monoxide over Africa with NCAR CAM, Atmos. Chem. and Phys., 8, 6801–6812, 2008. 18661

Herzog, M., Graf, H.-F., Textor, C., and Oberhuber, J. M.: The effect of phase changes of water on the development of volcanic plumes, J. Volcanol. Geotherm. Res., 87, 55–74, 1998. 18668

Hourdin, F., Couvreux, F., and Menut, L.: Parameterisation of the dry convective boundary layer based on a mass flux representation of thermals, J. Atmos. Sci., 59, 1105–1123, 2002. 18662, 18663

Hourdin, F., Musat, I., Bony, S., Braconnot, P., Codron, F., Dufresne, J.-L., Fairhead, L., Filiberti, M.-A., Friedlingstein, P., Grandpeix, J.-Y., Krinner, G., LeVan, P., Li, Z.-X., and Lott, F.: The LMDZ4 general circulation model: climate performance and sensitivity to parametrized physics with emphasis on tropical convection , Clim. Dynam., 27, 787–813, 2006. 18662, 18674

Jost, H.-J., Drdla, K., Stohl, A., et al.: In-situ observations of mid-latitude forest fire plumes deep in the stratosphere, Geophys. Res. Lett., 31, L11101, doi:10.1029/2003GL019253, 2004. 18661

Justice, C. O., Giglio, L., Korontzi, S., Owens, J., Morisette, J. T., Roy, D., Descloitres, J., Alleaume, S., Petitcolin, F., and Kaufman, Y.: The MODIS fire products, Remote Sens. Environ., 83, 244–262, 2002. 18673

Kahn, R. A., Li, W.-H., Moroney, C., Diner, D. J., Martonchik, J. V., and Fishbein, E.: Aerosol source plume physical characteristics from space-based multiangle imaging, J. Geophys. Res., 112, D11205, doi:10.1029/2006JD007647, 2007. 18660

Kaiser, J. W., Hollingsworth, A., Calvet, J.-C., Leroy, M., Tinz, M., and Desaubies, Y.: Harmonised coordination of atmosphere, land, and ocean ("HALO") integrated projects of the GMES backbone, 2009. 18661

Korontzi, S., Justice, C. O., and Scholes, R. J.: Influence of timing ans spatial extent of savanna fires in southern Africa on atmospheric emissions, J. Arid Environ., 54, 395–404, 2003. 18673

Liousse, C., Guillaume, B., Grégoire, J.-M., Mallet, M., Galy, C., Pont, V., Solmon, F., Poirson, A., Rosset, R., Serca, D., Mariscal, A., Dungal, L., Yoboué, V., Bedou, X., Konaré, A., Granier, C., Mieville, A., and van Velthoven, P.: Western African Aerosols Modeling with real time biomass burning emission inventories in the frame of AMMA-IDAF program, submitted to Atmos. Chem. Phys. Discuss., 2009. 18674, 18696

Louis, J.-F.: A parametric model of vertical eddy fluxes in the atmosphere., Bound.-Lay. Meteorol., 17, 187–202, 1979. 18674

Luderer, G., Trentmann, J., Winterrath, T., Textor, C., Herzog, M., Graf, H.-F., and Andrea, M. O.: Modeling of biomass smoke injection into the lower stratosphere by a large forest fire (Part II): Sensitivity studies, Atmos. Chem. Phys., 6, 5261–5277, 2006, http://www.atmos-chem-phys.net/6/5261/2006/. 18662, 18668, 18669, 18671

Morcrette, J. J.: Sur la paramétrisation du rayonnement dans les modèles de la circulation générale atmosphérique, thèse de Doctorat d'Etat, Univ. des Sci. et Tech. de Lille, France,

Modelling of pyro-convection

C. Rio et al.

Printer-friendly Version

Interactive Discussion

1984. 18674

Oberhuber, J. M., Herzog, M., Graf, H.-F., and Schwanke, K.: Volcanic plumensimulation on large scales, J. Volcanol. Geotherm. Res., 87, 29–53, 1998. 18668

Rio, C. and Hourdin, F.: A thermal plume model for the convective boundary layer: Representation of cumulus clouds, J. Atmos. Sci., 65, 407–425, 2008. 18662, 18663, 18667, 18680

Schultz, M. G., Woster, M., and et al: Power Product derived from Meteosat 8/9 and Identification of Operational User Needs, EUMETSAT contract EUM/CO/06/4600000277/YG, 2008. 18682

Siebesma, A. and Holtslag, A.: Model impacts of entrainment and detrainment rates in shallow cumulus convection, J. Atmos. Sci., 53, 2354–2364, 1996. 18667, 18668

Stocks, B. J., van Wilgen, B. W., Trollope, W. S. W., McRae, D. J., Mason, J. A., Weirich, F., and Potgieter, A. L. F.: Fuels and fire behavior dynamics on large-scale savanna fires in Kruger National Park, South Africa, J. Geophys. Res., 101, 23541–23550, doi:10.1029/95JD01734, 1996. 18662, 18669, 18670

Tiedtke, M.: A comprehensive mass flux scheme for cumulus parameterization in large-scale models, Mon. Weather Rev., 117, 1179–1800, 1989. 18668

Trentmann, J., Andreae, M. O., Graf, H.-F., Hobbs, P. V., and Ottmar, R. D.: Simulation of a biomass-burning plume: Comparison of model results with observations, J. Geophys. Res., 107, 4013, doi:10.1029/2001JD000410, 2002. 18668

Trentmann, J., Luderer, G., Winterrath, T., Fromm, M. D., Servranckx, R., Textor, C., Herzog, M., Graf, H.-F., and Andrea, M. O.: Modeling of biomass smoke injection into the lower stratosphere by a large forest fire (Part I): Reference simulation, Atmos. Chem. Phys., 6, 5247–5260, 2006, http://www.atmos-chem-phys.net/6/5247/2006/. 18662, 18668, 18669, 18689

Van der Werf, G. R., Randerson, J. T., Giglio, L., Collatz, G. J., Kasibhatla, P. S., and Arellano Jr., A. F.: Interannual variability in global biomass burning emissions from 1997 to 2004, Atmos. Chem. Phys., 6, 3423–3441, 2006, http://www.atmos-chem-phys.net/6/3423/2006/. 18660

Wooster, M. J., Roberts, G., and Perry, G. L. W.: Retrieval of biomass combustion rates and totals from fire radiative power observations: FRP derivation and calibration relationships between biomass consumption and fire radiative energy release, J. Geophys. Res., 110, D24311, doi:10.1029/2005JD006318, 2005. 18682

Modelling of pyro-convection

C. Rio et al.

Full Screen / Esc

Printer-friendly Version

Interactive Discussion

Table 1. Comparison of plume characteristics (injection height, virtual potential temperature excess, maximum vertical velocity and cloud base) as obtained with the ATHAM high resolution model in Trentmann et al. (2006) and with the pyro-thermal plume model.

	Trentmann et al. (2006)	pyro-thermal
z_{max}	12 000 m	10 200 m
θ_0'	40 K	44 K
w_{max}	40 m s^{-1}	40 m s^{-1}
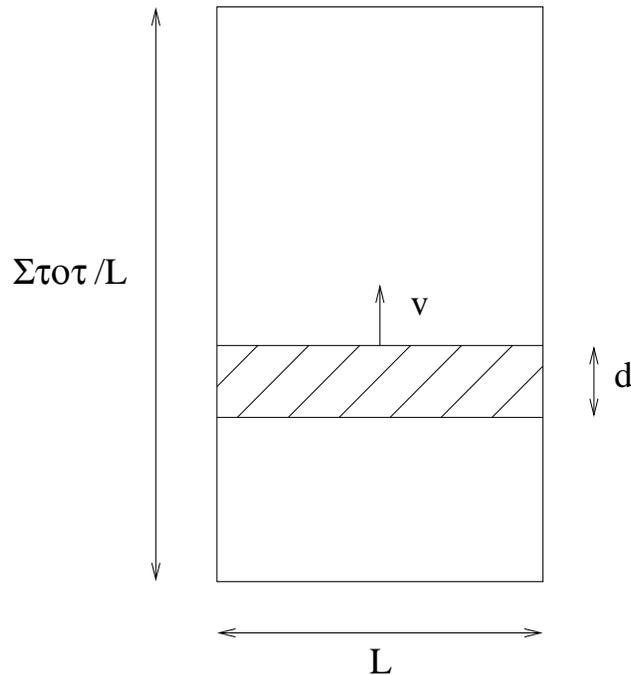
Fig. 1. Schematic view of the propagation of an idealized fire. The rectangular front of width *L* and depth *d* propagates at speed *v*.
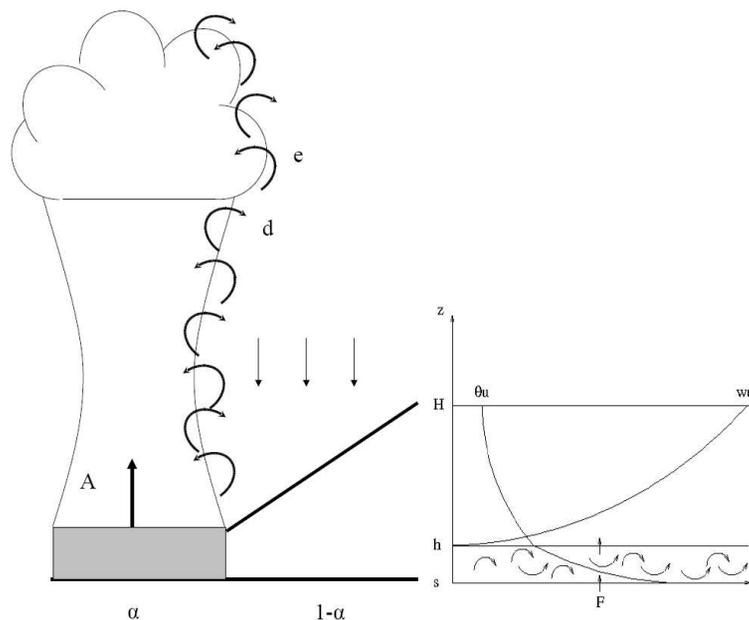
Fig. 2. Schematic view of the pyro-thermal generated by a fire (left) and zoom on the feed layer (right): diffusion is dominant in a layer h near surface while transport by thermals is dominant above. The plume covers a fraction α of the grid cell and is generated by the excess of temperature induced by fires leading to a vertical velocity w_u, a potential temperature θ_u and a mass-flux A at the top of the feed layer of height H. The plume mixes with environmental air at each level at rates e and d.
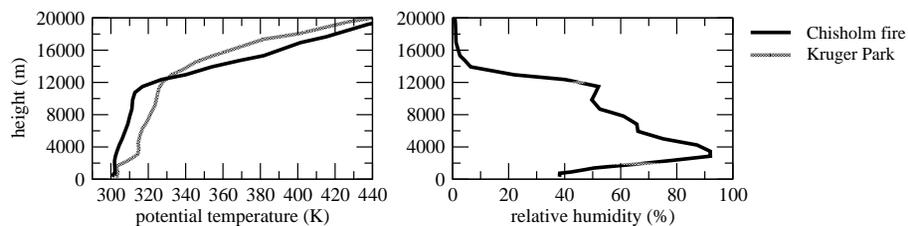
Fig. 3. Meteorological conditions, potential temperature in K and relative humidity in % at two fire locations: 55 N/114 W the 28th of May 2001 at 16:30 LT for the Chisholm fire and 25 S/31 E the 24th of September 1992 at 14:00 LT for the Kruger fire.
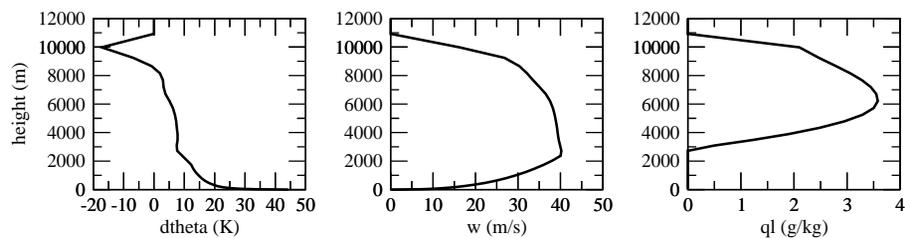
Fig. 4. Plume characteristics above the Chisholm fire: virtual potential temperature excess (K), vertical velocity (m s^{-1}) and cloudy liquid water (g kg^{-1}).
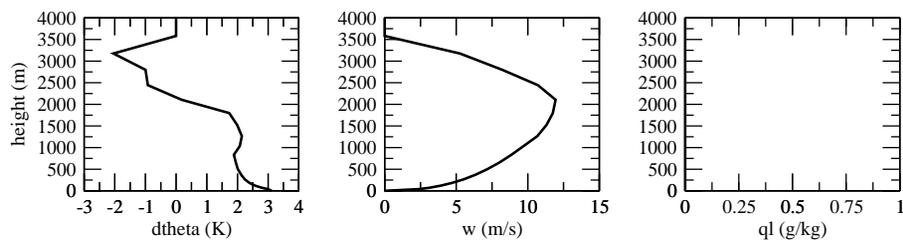
Fig. 5. Plume characteristics above the Kruger fire: virtual potential temperature excess (K), vertical velocity (m s^{-1}) and cloudy liquid water (g kg^{-1}).
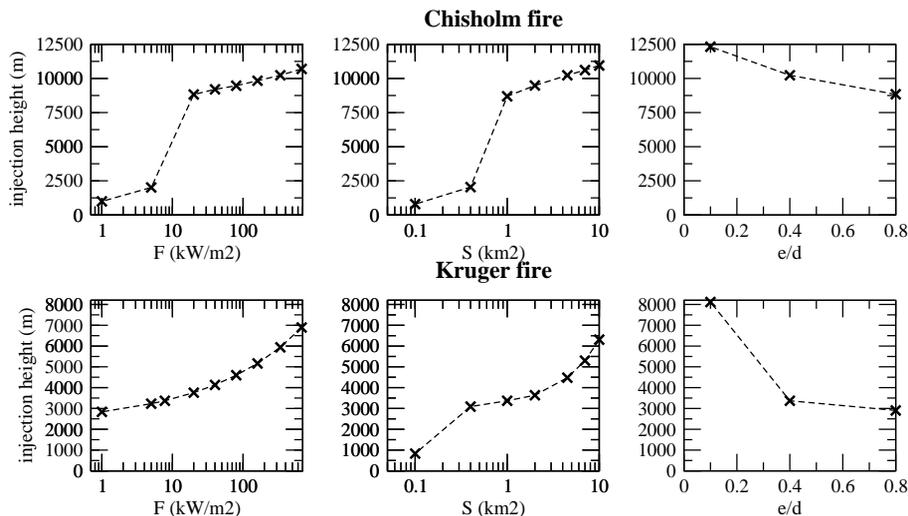
Fig. 6. Sensitivity of the injection height to the heat flux released (*F*), the active burning surface (*S*), and the ration e/d for the Chisholm fire (top) and Kruger fire (bottom) conditions.
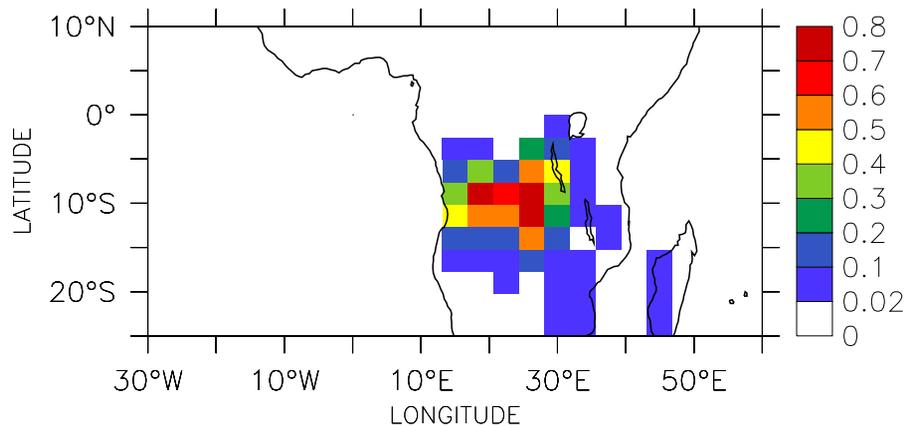
Fig. 7. CO_2 emissions from biomass burning in $kg\,m^{-2}\,day^{-1}$ in July 2006 over Southern Africa derived from observations conducted during the AMMA field campaign (Liousse et al., 2009)
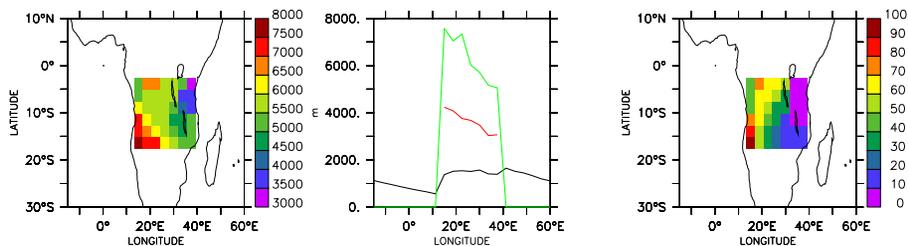
Fig. 8. Injection height of CO_2 emissions: Maximal injection height (m) simulated between the 10th and the 30th of July (left); maximal injection height (green), mean injection height of emissions injected above the boundary layer height (red), and mean boundary layer height (dark) averaged between 5 and 20S over 20 days of simulation in July (middle); percentage of time at which, the injection height being greater than 2 km, emissions are injected higher than 4 km (right).
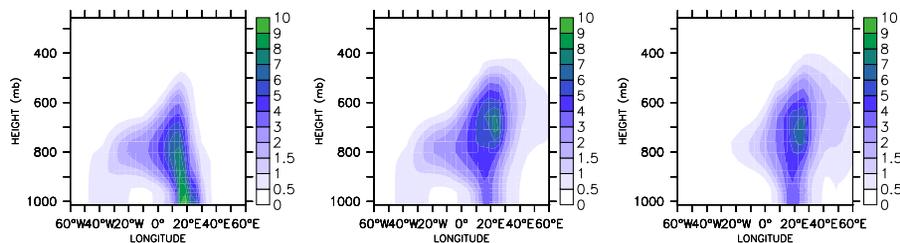
Fig. 9. Vertical distribution of CO_2 concentration in ppmv averaged between 5 and 20S over the 20 last days of July for simulations REF (left), TH (middle) and TH with $\beta = 0.1$ (right).
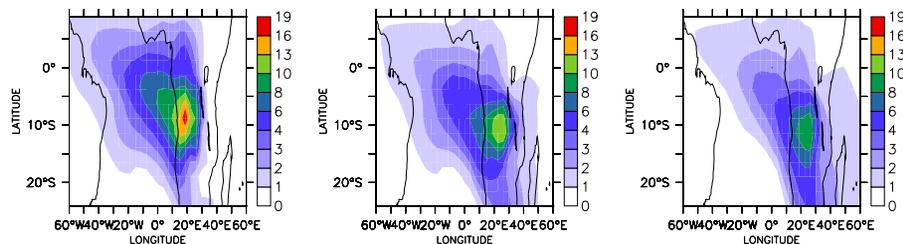
Fig. 10. Peak of the CO_2 concentration vertical distribution averaged over the 20 last days of July for simulations REF (left), TH (middle) and TH with $\beta = 0.1$ (right).

Full Screen / Esc

Printer-friendly Version

Interactive Discussion
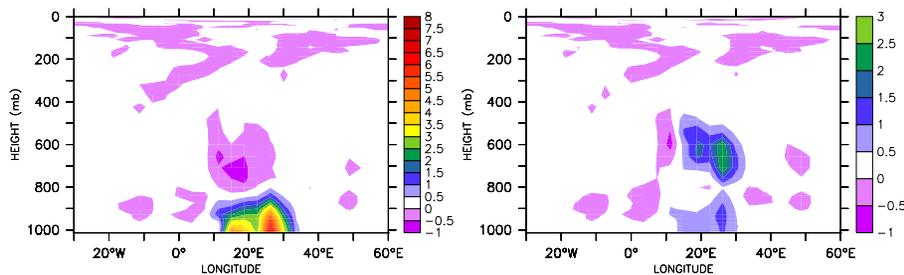
Fig. 11. Vertical section of the amplitude of the diurnal cycle of CO_2 (ppmv) averaged between 5S and 20S over the 20 last days of July for simulation REF (left) and TH (right).
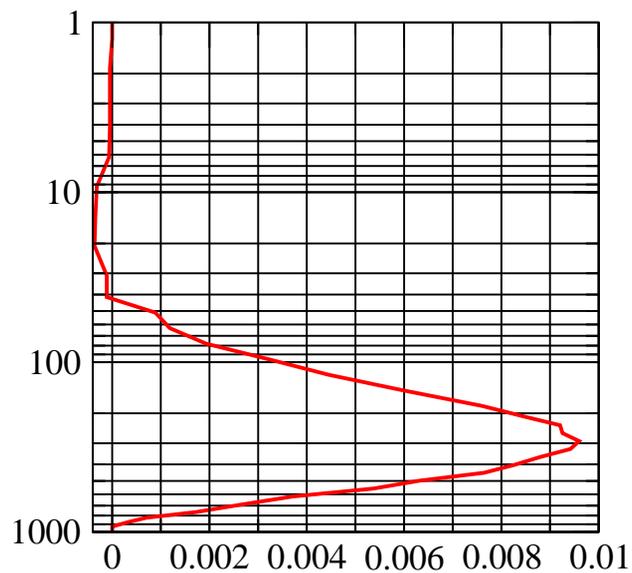
Fig. 12. Weighting function of CO_2 column satellite as determined by Chédin et al. (2003).
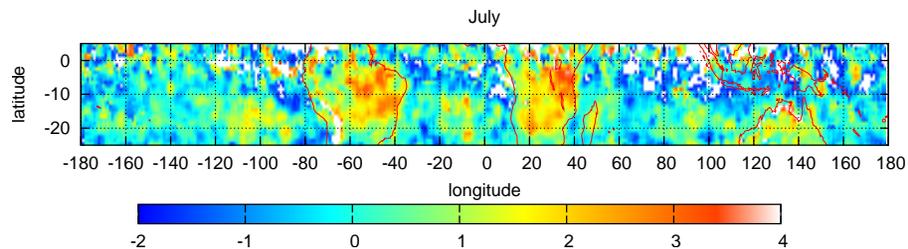
Fig. 13. Daily Tropospheric Excess (ppmv) in July retrieved from satellite measurements by Chédin et al. (2003).
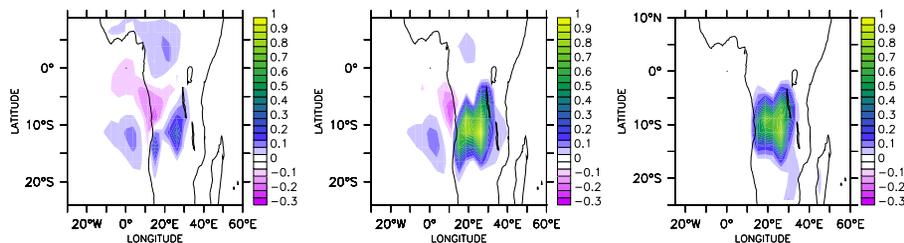
Fig. 14. Daily Tropospheric Excess of CO_2 (ppmv) in July as simulated by simulations REF (left) and TH (middle) and estimated from CO_2 emissions by assuming a uniform distribution of CO_2 emissions between 800 and 500 hPa (right).
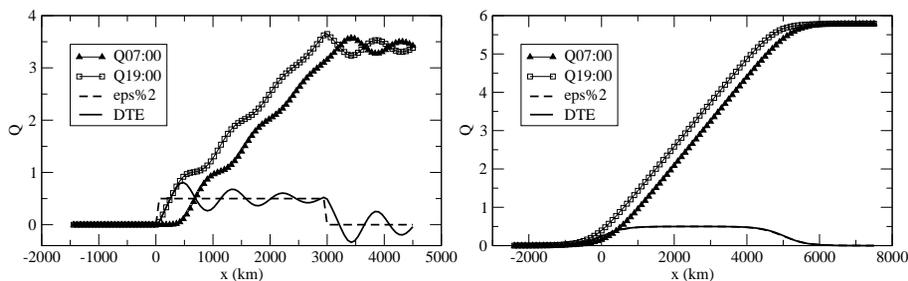
Fig. 15. DTE computation for a fire injecting emissions along $x = [0, L]$ in the presence of 1-D advection with a constant wind $U = 10$ m/s for $L = 3000$ km ($L/(U\delta t)=3$) considering a top-hat source region (left) and $L = 6000$ km ($L/(U\delta t) = 6$) considering smoothed emissions (right). Results are presented for day 29 with concentrations at 07:00 just before fire injection (black triangles) and at 19:00, just after fire injection (white squares). The DTE (difference between the two previous curves, dashed) is compared to half the emission $\varepsilon/2$ (dashed curve).

Modelling of pyro-convection

C. Rio et al.

Full Screen / Esc

Printer-friendly Version

Interactive Discussion
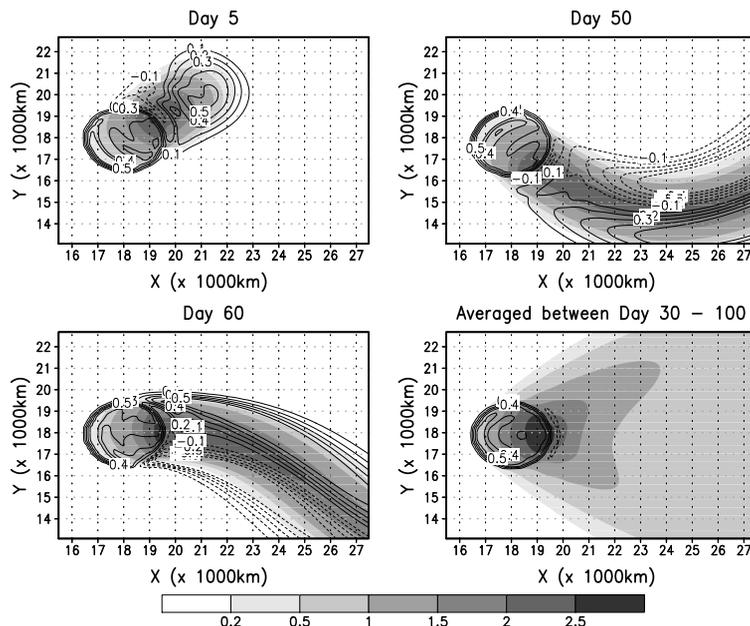
Fig. 16. DTE computation for a fire injecting emissions inside a circle of diameter L = 3000 km in the presence of constant advection over the domain at a given time. At time t, the wind in the x and y direction is respectively $U = U_0 \sqrt{(1. + \cos(2\pi t/\tau)^2)}/\sqrt{(2)}$ and $V = U_0 \sin(2\pi t/\tau)/\sqrt{(2)}$ with $U_0 = 10$ m/s. $\tau = 1.25\pi\delta t$ is chosen so that the oscillation of wind is not in phase with the diurnal cycle. On each panel, the concentration is shown (shaded) together with the associated DTE contours (−0.5, −0.4, −0.3, −0.2, −0.1, 0.1, 0.2, 0.3, 0.4, 0.5).